Chinese Chemical Letters 34 (2023) 108223

Contents lists available at ScienceDirect

Chinese Chemical Letters

journal homepage: www.elsevier.com/locate/cclet

Engineering *J*-aggregates for NIR-induced *meso*-CF_3-BODIPY nanoparticles by activated apoptosis mechanism in photothermal therapy

Chujing Ye[a,1], Shan Zhang[b,1], Dongxiang Zhang[a,1], Yue Shen[a], Zhan Wang[b], Huan Wang[b], Junyi Ren[b], Xin-Dong Jiang[a,*], Jianjun Du[c,*], Rong Shang[d], Guiling Wang[b,*]

[a] *Liaoning & Shenyang Key Laboratory of Functional Dye and Pigment, Shenyang University of Chemical Technology, Shenyang 110142, China*
[b] *Department of Cell Biology, China Medical University, Shenyang 110122, China*
[c] *State Key Laboratory of Fine Chemicals, Dalian University of Technology, Dalian 110624, China*
[d] *Department of Chemistry, Graduate School of Science, Hiroshima University, Higashi-Hiroshima 7398526, Japan*

ARTICLE INFO

Article history:
Received 27 November 2022
Revised 6 February 2023
Accepted 10 February 2023
Available online 15 February 2023

Keywords:
NIR dye
J-aggregate
CF_3-BODIPY
Photothermal therapy
Cell apoptosis

ABSTRACT

Forming *J*-aggregates by organic monomer is a fascinating strategy to urge spectroscopic redshift with respect to that of the monomer. Herein, we designed 1,7-diphenyl-substituted ***meso*–CF_3-BDP** monomer confirmed by X-ray crystallographic analysis. The low-barrier rotation of the –CF_3 group in ***meso*–CF_3-BDP 1** significantly enhances the non-radiative efficiency, and the photothermal conversion efficiency (PCE) of the self-assembled nanoparticles (**1-NPs**: $\lambda_{abs} = 746$ nm) by *J*-aggregates was 82%. **1-NPs** could effectively block cell cycle progression, inhibit cancer cell proliferation and trigger cell apoptosis under low power laser irradiation (0.2 W/cm^2). This study proposes an alternate molecular design platform by *J*-aggregates to promote PCE through the insertion of rotating segment and trigger the cancer cells apoptosis in photothermal therapy at low power laser density.

Cancer phototherapy refers to the utilization of photon-energy to implement the tumor ablation, mainly involving photodynamic therapy (PDT) and photothermal therapy (PTT), which had been emerged as cancer treatment approach following surgery, chemotherapy and radiotherapy. Compared with other cancer therapies, phototherapy holds great promise for precisely navigating at the lesion site for diagnostic therapy, non-tissue invasiveness, high treatment efficiency and anti-drug resistance [1–6]. Strong absorption of the near-infrared (NIR) photon with high penetration of tissue, and efficient conversion to heat energy through non-radiative decay are critical factors for constructing photothermal agents (PTAs) [7–13]. Compared with the molecular engineering strategy of extending π-π conjugated structure or inserting electron-donating/withdrawing groups, the *J*-aggregate by organic monomer endowed it attractively optical properties, such as spectroscopic bathochromic shift, high photobleaching resistance, strong light-harvesting feature [14–18]. *J*-aggregates demand slip-stacked alignment ($\theta < 54.7°$), but currently there are few reports about *J*-aggregates of cyanine, chlorophyll, perylenediimide, squaranine dye and borondipyrromethene (BODIPY or BDP) [19–23]. Owing to the excellent spectral characters of BODIPY, such as high molar extinction coefficients, outstanding photostability and easy modification, it is urgent to conduct a thorough analysis for the crystal aggregation structure of BODIPY, and explore light-induced application, especially in the field of biomedical therapeutics [24–27].

In contrast with PDT, PTT is not restricted by the hypoxic of the tumor microenvironment. Whereas, PTT usually undergoes the necrosis, which may impair the treatment outcomes by triggering pro-inflammatory responses and promoting tumor growth [8]. By molecular design and photoexcitation condition, PTT can also be modulated to induce apoptosis rather than necrosis, which is significative since apoptosis prevented an inflammatory response. Above all, PTT is an efficient, non-invasive treatment method that overcomes hypoxia restriction and inflammation [28]. The relaxed molecules in the lowest vibrational level of the excited state can undergo one or more of the three paths, that is, non-radiative transition, radiative transition (fluorescence emission) and intersystem crossing (ISC), to return to the ground state. In this regard, three pathways compete with each other, and it is pivotal to effectively inhibit the other two processes for improving non-radiative relaxation, which is conducive for PTT. In short, integrating high pho-

* Corresponding authors.
E-mail addresses: xdjiang@syuct.edu.cn (X.-D. Jiang), dujj@dlut.edu.cn (J. Du), glingwang@cmu.edu.cn (G. Wang).
[1] These authors contributed equally to this work.

https://doi.org/10.1016/j.cclet.2023.108223
1001-8417/

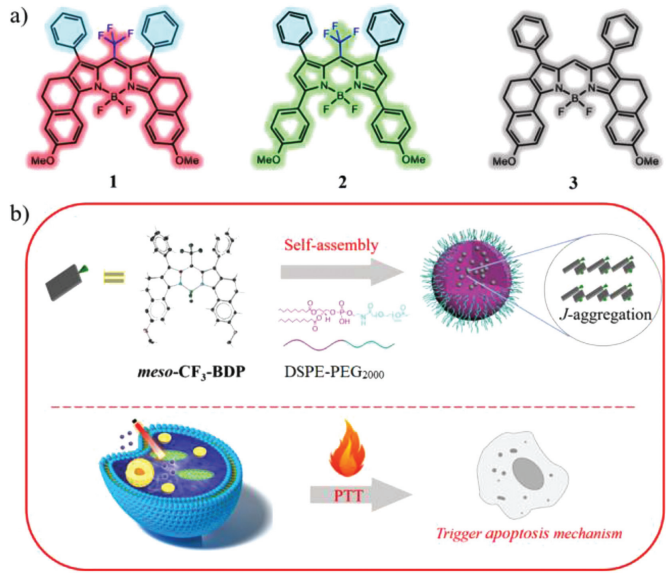

Fig. 1. (a) Structures for **BDPs 1–3**. (b) Design strategies of self-assembling nanoparticles and application of light triggering apoptosis.

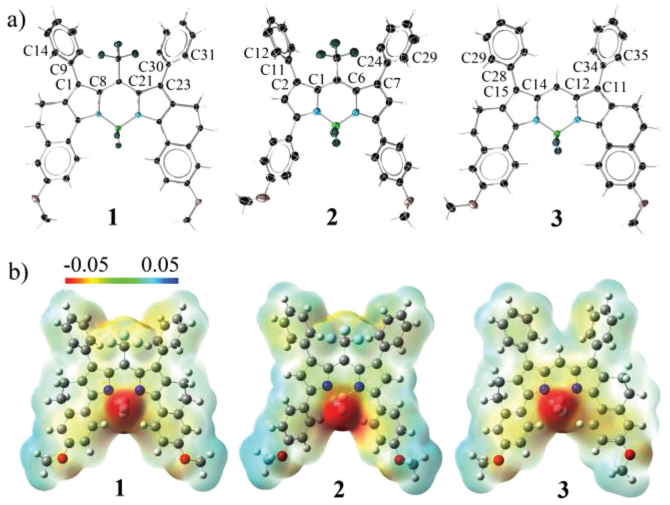

Fig. 2. (a) ORTEP drawing of **BDPs 1–3** (CCDC: 2189483 for **1**; 1547540 for **2** [36]; 2189484 for **3**). The dihedral angles: C14-C9-C1-C8: 126.4(3)°, C31-C30-C23-C21: 134.7(3)° for **1**; C12-C11-C2-C1: 107.1(5)°, C29-C24-C7-C6: 125.2(6)° for **2**; C29-C28-C15-C14: 137.6(3)°, C35-C34-C11-C12: 134.3(3)° for **3**. (b) ESP distribution diagram of **BDPs 1–3**.

tothermal conversion efficiency (PCE), deep tissue penetration and excellent photostability for the ideal PTAs are vital [29–33].

To enhance PCE, researchers constructed various structural BODIPYs, which are often involved in intramolecular charge transfer (ICT), photoinduced electron transfer (PET), rotating segments and so forth. For instance, Ma *et al*. showed a BODIPY-based PTA, enhanced phototherapeutic performance of which is resulted from the reduction of radiation transition by ICT [34]. Based on PET to quench the fluorescence, Huang *et al*. reported dimethylamino-substituted aza-BODIPY with a moderate PCE ($\eta = 35\%$) [35]. Especially, the low-barrier rotation strategy of a bulky group (such as $-CF_3$, $-t$Bu) is employed to directly promote non-radiative decay. In 2017, our group prepared NIR-absorbing *meso*–CF_3-BODIPYs by one-pot synthesis for the first time and reveal the property of non-fluorescent emission [36]. In 2019, Xi *et al*. successfully discovered the highest PCE ($\eta = 88.3\%$) of this *meso*–CF_3-BODIPY [37]. Very recently, our group successfully synthesized 1,7-di–*tert*–butyl–substituted aza-BODIPY for the first time [38]. Although the low-barrier rotation of the distal $-t$Bu groups in aza-BODIPY results in low quantum yield, the PCE ($\eta = 48\%$) is remarkably enhanced [38]. Thereby, by restricting fluorescence and ISC, the enhancement of PCE could be achieved by high-efficiency non-radiative decay [39]. Herein, to understand the influence of the $-CF_3$ rotation effect on non-radiation attenuation profoundly, 1,7-diphenyl-substituted *meso*–CF_3-BODIPY (namely ***meso*–CF_3-BDP**) was designed (Fig. 1a). The crystal structure showed obvious slip-stacked alignment ($\theta = 24°$), and the dye nanoparticles constituted by self-assembly emerged obvious bathochromic-shift ($\lambda_{abs} = 746$ nm) due to *J*-aggregates. In addition, the low-barrier rotation of the $-CF_3$ group can directly promote non-radiative decay. Self-assembled ***meso*–CF_3-BDP 1** nanoparticles (namely **1-NPs**) showed excellent PCE ($\eta = 82\%$), which is highly desirable for an effective and potential tumor PTA. Although the photothermal radiation with different photon intensity is acquainted by trigger cell death through either necrosis or apoptosis [40], PTT is usually engaged in necrosis mechanism. In contrast, PTT caused by apoptosis pathway is rarely reported [40,41]. Furthermore, based on American National Standard for Safe Use of Lasers Outdoors, the maximum permissible exposure (MPE) for skin exposure is 0.2 W/cm^2 at the 635 nm laser. Hence, the safe PTT at low power laser density should be advocated and could be involved in the apoptosis mechanism. In this work, **1-NPs** fabricated by *J*-aggregates could induce the cancer cells death at low laser power density by triggering the apoptosis mechanism, which is fascinating since apoptosis discourages an inflammatory response (Fig. 1b). As a result, this study proposes an alternate molecular design platform by *J*-aggregates to enhance PCE through the insertion of rotating segment ($-CF_3$) and trigger the cancer cells apoptosis in PTT under low power laser irradiation.

Based on the synthetic method pioneered by our group [36], one-pot synthesis of ***meso*–CF_3-BDP 1** is achieved in 43% yields, as shown in Scheme S1 (Supporting information). In a sharp contrast, the contrastable dye ***meso*–H-BDP 3** (H-substitute at *meso*–site) was also prepared (Scheme S1 and Figs. S1–S5 in Supporting information). Moreover, the solid state structures of **BDPs 1–3** were confirmed by X-ray crystallographic analysis (Fig. 2a). The sp^3 hybridized boron center in ***meso*–CF_3-BDP 1** appeared as slightly distorted tetrahedron geometry with angles N1-B1-N2 of 108.15(19)° and F1-B1-F2 of 111.2(2)°, deviating from the ideal value of 109.5° In a stark comparison with ***meso*–H-BDP 3** (the dihedral angles of C29-C28-C15-C14: 137.6°; C35-C34-C11-C12: 134.3°), the dihedral angles of C14-C9-C1-C8 and C31-C30-C23-C21 in ***meso*–CF_3-BDP 1** were small and measured to be 126.4° and 134.7°, respectively. Moreover, the smaller dihedral angles of C12-C11-C2-C1 and C29-C24-C7-C6 in ***meso*–CF_3-BDP 2** (non-ring-fused configuration) were also observed to be 107.1° and 125.2°, respectively [36]. Therefore, the 1,7-diphenyl torsion is mainly due to the steric hindrance from the introduction of the *meso*–CF_3 group, which meanwhile provides the enough space for the rotation of the $-CF_3$ group at *meso*–site. Moreover, the electrostatic potential (ESP) maps for **1–3** in the gas phase were also investigated (Fig. 2b). The negative charges (red color) were mainly concentrated on the fluorine atoms and oxygen atoms of BODIPY units, including the $-CF_3$ group. In contrast, the positive charges (blue color) were evenly distributed in the remaining positions. These results demonstrated the uneven charge distribution and the significant structural distortion of BODIPY, which is beneficial for the rotation energy-releasing of the $-CF_3$ group.

To gain insight into the photophysical properties of ***meso*–CF_3-BDPs**, the absorption and emission spectra for **BDPs 1–3** were measured and outlined in Fig. 3a and Table S1 (Supporting information). Compared to the spectroscopic information for corre-

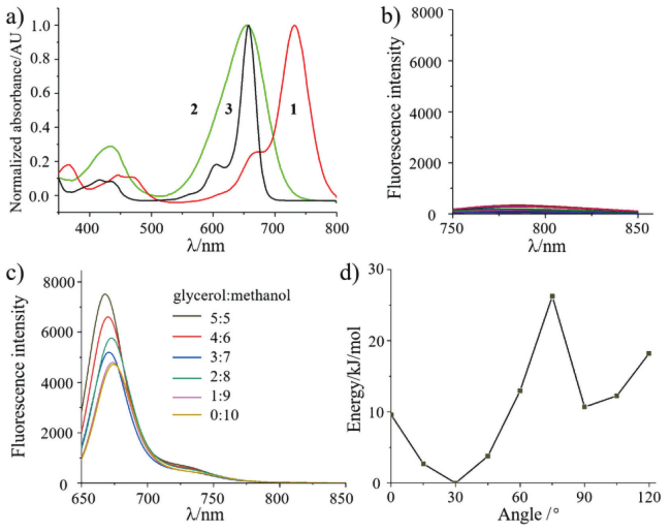

Fig. 3. (a) Normalized absorption spectra of **BDPs 1** (red), **2** (green) and **3** (black) in CH_2Cl_2 at 298 K. (b, c) Emission changes of BDPs **1** and **3** in different concentrations of glycerol/methanol (v/v: 0:10; 1:9, 2:8, 3:7, 4:6 and 5:5) solution. (d) Energy levels of the S_0 states of chemical bond for **BDP 1** with the dihedral angle θ (Scheme S1).

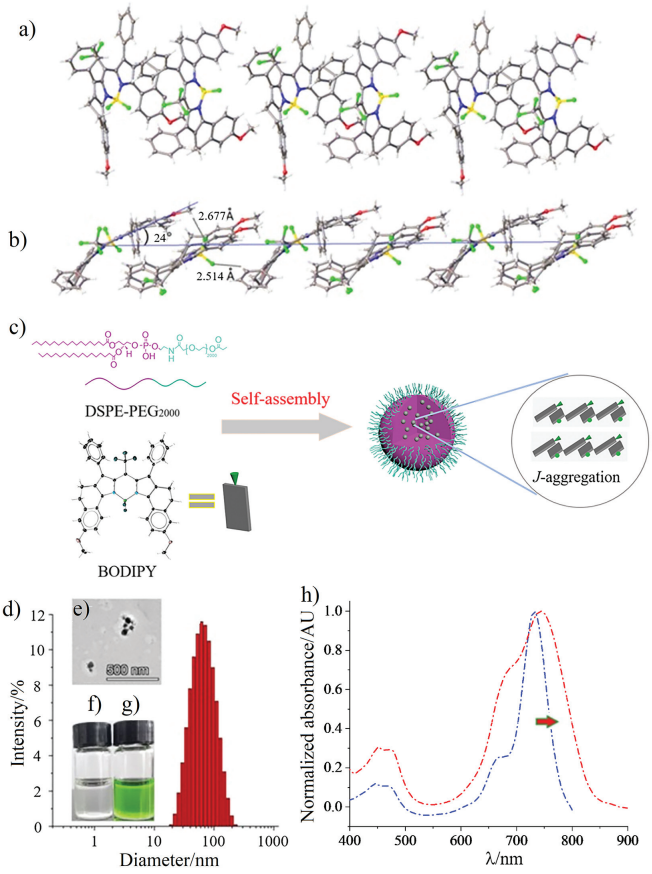

Fig. 4. Molecular packing diagram of (a) front view and (b) side view for ***meso*–CF_3-BDP 1**. (c) Self-assembly of ***meso*–CF_3-BDP 1**. (d) DLS and (e) TEM of **1-NPs** in aqueous solution. (f) Photo of pure water. (g) Photo of **1-NPs** in water. (h) Normalized absorption of 5 μmol/L ***meso*–CF_3-BDP 1** (blue curve) in CH_2Cl_2 and 20 μmol/L **1-NPs** in water (red curve).

sponding dye ***meso*–H-BDP 3** ($\lambda_{abs}/\lambda_{em} = 658/687$ nm, $\phi_f = 0.55$), the introduction of the electron-withdrawing group ($-CF_3$) leads to a remarkable bathochromic shift (74 nm) of ***meso*–CF_3-BDP 1** ($\lambda_{abs} = 732$ nm), the absorption maximum of which locates at the NIR region. However, ***meso*–CF_3-BDP 1** was astoundingly found to exhibit no fluorescence character. The lack of fluorescence signal indicates the excited state decays through non-radiative pathways and results in highly efficient PCE. In comparison with ***meso*–H-BDP 3** ($\varepsilon = 140{,}000$ L mol^{-1} cm^{-1}; FWHM: 36 nm), ***meso*–CF_3-BDP 1** has higher molar extinction coefficients (155,000 L mol^{-1} cm^{-1}) and wider full width at half maxima (FWHM: 52 nm) which is mainly caused by the drastic vibration of the $-CF_3$ fragment. Additionally, the band gaps (LUMO/HOMO) were calculated to be 2.07, 2.23 and 2.30 eV for **BDPs 1–3**, respectively (Fig. S6 in Supporting information). All the theoretical calculation results well explained and supported the difference of absorption maxima. Furthermore, in order to reveal the obstruction of the rotating segment, the effect of viscosity on the fluorescence by using different concentrations of glycerol was further investigated (Figs. 3b and c). Generally, the substituent rotation can be leastwise restricted in viscous media, and the corresponding fluorescence enhancement should be observed [42–45]. Comparing to the remarkable fluorescence enhancement of ***meso*–H-BDP 3**, no obvious change in fluorescence intensity was observed for ***meso*–CF_3-BDP 1** in the mixture of glycerol and methanol in different proportions (Figs. 3b and c). This was attributed to the "low-barrier" rotation of the $-CF_3$ group (Fig. S7 in Supporting information). Comparing to ***meso*–H-BDP 3**, the smaller dihedral angles in ***meso*–CF_3-BDP 1** dodges the steric hindrance between the 1,7-diphenyl groups and the *meso*–CF_3 group to exactly provide the space for the low-barrier rotation of the $-CF_3$ group (Fig. 2a). Moreover, we also calculated the rotated potential energy barrier of the $-CF_3$ group in ***meso*–CF_3-BDP 1**, as picked in Fig. 3d. The energy maxima in ***meso*–CF_3-BDP 1** are 26.3 kJ/mol, indicating the low-barrier rotation of the $-CF_3$ group in this molecule. As a result, the $-CF_3$ rotation in ***meso*–CF_3-BDP 1** significantly increases the non-radiative efficiency.

We further investigated singlet oxygen generation of ***meso*–CF_3-BDPs 1** and **2** to inspect the ISC process. By utilizing 1,3-diphenylisobenzofuran (DPBF), a singlet oxygen ($^1O_2$) indicator, the efficiency of $^1O_2$ generation was evaluated by detecting the decrease of DPBF indicator absorbance at 416 nm [46,47]. Based on the slope coefficient of the decay lines, the $^1O_2$ yields of ***meso*–CF_3-BDPs 1** and **2** were so low and calculated to be 0 and 0.006 respectively (Fig. S8 in Supporting information), indicating that ISC is basically prohibited.

Since we preliminarily probed the key data of fluorescence ($\phi_f = 0$) and $^1O_2$ yield ($\phi_\Delta = 0$) of this novel dye ***meso*–CF_3-BDP 1**, such information urges us to further explore the insight into the photothermal conversion capacity. To enhance the water solubility and biocompatibility of ***meso*–CF_3-BDP 1** for application in photoimaging and phototherapy in biological system, ***meso*–CF_3-BDP 1** and amphipathic polymer material 1,2-distearoyl-*sn*–glycero-3-phosphoethanolamine-*N*-[methoxy(polyethylene glycol)–2000] (DSPE-PEG_{2000}) were self-assembled into dye nanoparticles (abbreviated **1-NPs**) [48–50]. To confirm the molecular design concept, the molecular packing mode of ***meso*–CF_3-BDP 1** *via* single-crystal structure analysis was firstly investigated (Fig. 4a). In the single-crystal structure, the C–H···F hydrogen bond (2.677 Å) between the –OMe group and the $-BF_2-$ group, and the C–H···F hydrogen bond (2.514 Å) between the –Ph group and the $-BF_2-$ group dominate the molecular packing structure of ***meso*–CF_3-BDP 1** (Fig. 4b), which facilitates the *J*-aggregation packing mode. The slipping angle and the distance between each molecule are determined to be 24° and ~3.6 Å, respectively (Fig. 4b). Based on transmission electron microscopy (TEM) photograph, their sizes were less than 110 nm (Fig. 4e). Moreover, dynamic light scattering (DLS) of **1-NPs** showed a suitable hydrodynamic diameter (10–110 nm) in Fig. 4d, and the average hydrodynamic diameter and the polydispersity index (PDI) were about

56.35 nm and 0.215. The prepared **1-NPs** in aqueous solution are stable for two weeks (Figs. 4f and g). Owing to the *J*-aggregation effect (Fig. 4c), the absorption maximum ($\lambda_{abs} = 746$ nm) of **1-NPs** in aqueous solution bathochromically shifted 14 nm and its absorption band covered the ranges of the NIR region (650–900 nm) and became wider [14,17], comparing to those (650–800 nm) of **1** in CH_2Cl_2 (Fig. 4h) [51].

To discover the photothermal efficacy of hydrosoluble **1-NPs** (Figs. S9 and S10 in Supporting information), the temperature elevation of the multiple concentrations ranging from 20 μmol/L to 80 μmol/L **1-NPs** were recorded in the presence of 690 nm laser irradiation (0.6 W/cm^2) (Fig. S9a). As revealed in Figs. S9a and b, 80 μmol/L **1-NPs** exhibited a intense photothermal conversion ability ($\Delta T = 55.5$ °C) upon photon-irradiation (0.6 W/cm^2 in 5 min), comparing to those ($\Delta T = 27.5$ °C for 20 μmol/L; $\Delta T = 36.1$ °C for 40 μmol/L) in the low concentration, suggesting that temperature augment is concentration dependent. Thus, we further discussed the temperature enhancement under different illumination of 80 μmol/L **1-NPs**, and found that the stronger the radiation intensity, the higher temperature enhancement ($\Delta T = 28.9$ °C in 0.2 W/cm^2; $\Delta T = 39.4$ °C in 0.4 W/cm^2; $\Delta T = 55.5$ °C in 0.6 W/cm^2) (Fig. S9c). Therefore, higher concentration and stronger laser radiation are feasible for photothermal conversion process. **1-NPs** showed an outstanding photothermal conversion during three heating–cooling cycles, approving the possibility of reuse (Fig. S9d). The PCE of **1-NPs** was established by acquiring the temperature response of the heating and cooling curves (Fig. S9e), as revealed in Fig. S9f ($\tau = 129$ s). The PCE value (η) of **1-NPs** was calculated to be 82%, which was much higher than that of the commercialized PTAs indocyanine green (ICG) NPs (η = 17.3%) [52,53], Au nanorods (η = 21%) [54] and was inferior to the highest one (η = 88.3%) [37].

To further explore the biological compatibility and potential inhibiting cancer cells effect of **1-NPs**, the double-staining kit calcein AM (stains live cells with green fluorescence presented) and prodium iodide (PI, stains dead cells with red fluorescence presented) was applied to demonstrate the effectiveness of **1-NPs** with low-power photon-irradiation on cancer cell viability. As displayed in column 4 of Fig. S11 (Supporting information), **1-NPs** induced death of gastric cancer cells SGC-7901, exhibiting a significant red fluorescence, suggesting cell death state under laser treatment. In contrast, control group, sole laser-treated or sole **1-NPs**-treated groups had distinct green fluorescence, demonstrating no phototherapy effect for killing cancer cells. These results exhibited that cancer cells destroyed by **1-NPs** with laser irradiation (690 nm, 0.2 W/cm^2) was observed on the premise of ensuring biosafety.

To deeply research the triggering mechanism of **1-NPs** under photo-mediated on cancer cell death, then, flow cytometry on SGC-7901 cells was performed. In comparison to the other groups, the cells treated with **1-NPs** plus low power laser irradiation (690 nm, 0.2 W/cm^2) displayed a reduction in the stage of DNA synthesis phase (S phase), indicating that **1-NPs** intercepted cancer cell proliferation, block cancer cell cycle progression caused by laser irradiation, as shown in Fig. 5a [55–57]. Meanwhile, Fig. 5b evaluated that the percentage of apoptotic cells increased from 14.42% to 54.33% after treatment with **1-NPs** imposed laser irradiation, cells treated with **1-NPs** alone or light irradiation alone showed lower apoptosis rates, demonstrating the valid competence of **1-NPs** to induce cancer cells apoptosis under light-responsive. The effect of **1-NPs** with NIR laser irradiation on cycle and apoptosis related factors was further verified in SGC-7901 cancer cell by real-time polymerase chain reaction (RT-qPCR) and Western blot at both RNA and protein levels as shown in Figs. 5c and d and Fig. S12 (Supporting information). Over expression of Cyclin D1 resulted in cell cycle disorder and uncontrolled cancer cell growth, the decreased expression level of Cyclin D1 indicated that treatment with **1-NPs** plus 690 nm laser irradiation induced cancer cell cycle stagnation,

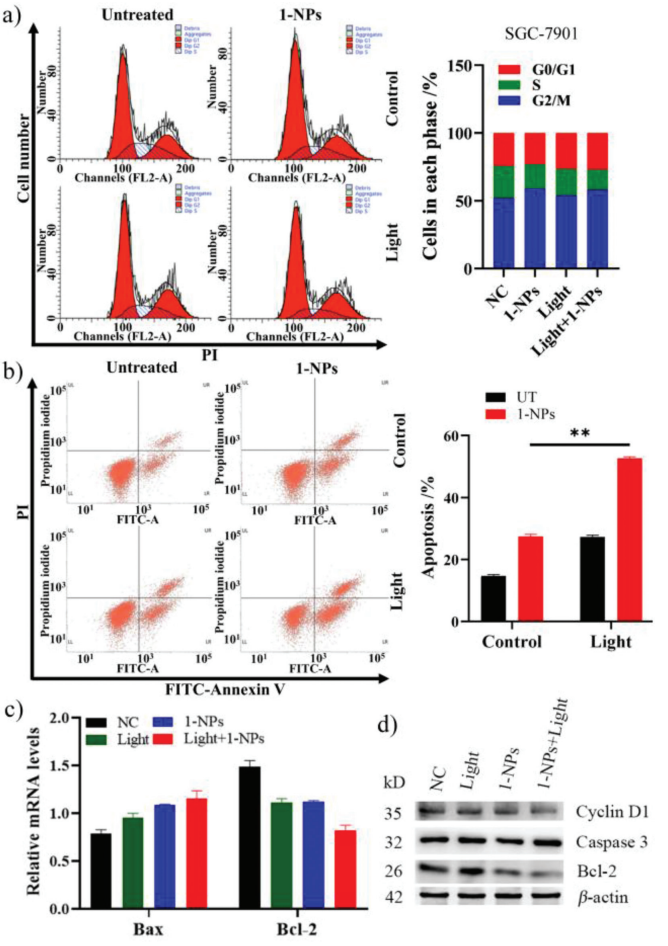

Fig. 5. (a) Cell cycle analysis using flow cytometry in SGC-7901 cells. NC: negative control. (b) Apoptosis analysis using flow cytometry in SGC-7901 cells. $^{**}P < 0.01$, $n = 2$. *t*-test. All data were shown as mean ± standard deviation (SD). UT: untreated. (c) mRNA expression levels related to the regulation of apoptosis (Bax and Bcl-2) was evaluated using RT-qPCR in SGC-7901 cells. (d) Protein expression levels related to the regulation of cell cycle (Cyclin D1) and cell apoptosis (Bax and Bcl-2) were evaluated by Western blot in SGC-7901 cells. Different treatments are including untreated, 20 μmol/L **1-NPs**, laser (690 nm, 20 min), and **BDP 1-NPs** plus laser irradiation (0.2 W/cm^2).

and suppressed cancer cell proliferation [58]. Meanwhile, Bcl-2 is a negative factor of cell apoptosis and Bax is a positive regulator of apoptosis [59,60]. As shown in Figs. 5c and d, executing light-treated in the **1-NPs** groups, the RNA and protein levels of Bax increased, while the RNA and protein levels of Bcl-2 decreased, indicating that the photothermal therapeutic effect of **1-NPs** can trigger apoptosis in cancer cells. The above results are in high consistency with those of AM/PI co-stained experiments, indicating that **1-NPs** upon low-power laser irradiation effectively restrains cell cycle progression, triggers cell apoptosis factors, and inhibits cancer cell proliferation. Thus, the design principle for **1-NPs** obtained the probability of a NIR PTA for cancer treatment.

In conclusion, one-pot synthesis of 1,7-diphenyl subsitituted ***meso*–CF_3-BDP** was achieved in 43% yields. The low-barrier rotation of the $-CF_3$ group in ***meso*–CF_3-BDP** remarkably increases the non-radiative efficiency, and the photothermal conversion efficiency of the self-assembled nanoparticles (**1-NPs**: $\lambda_{abs} = 746$ nm) by *J*-aggregates based on X-ray crystallographic analysis was 82%. **1-NPs** plus low power laser irradiation (0.2 W/cm^2) could effectively block cell cycle progression, inhibit cancer cell proliferation and trigger cell apoptosis. Therefore, this study proposes an alternate molecular design platform by *J*-aggregates to promote PCE

through the introduction of rotating segment and trigger the cancer cells apoptosis in PTT at low power laser density.

Declaration of competing interest

The authors declare no conflict of interest.

Acknowledgments

This work was supported by the National Natural Science Foundation of China (Nos. 22078201, U1908202), Natural Science Foundation of Liaoning (No. 2021NLTS1206), Serving Local Project of Education Department of Liaoning Province (No. LZ2020005), Liaoning & Shenyang Key Laboratory of Functional Dye and Pigment (Nos. 2021JH13/10200018, 21-104-0-23) and the Distinguished Professor Project Liaoning Province (No. 20183532).

Supplementary materials

Supplementary material associated with this article can be found, in the online version, at doi:10.1016/j.cclet.2023.108223.

References

[1] J. Li, M. Zhang, Y. Yang, et al., Chin. Chem. Lett. 32 (2021) 3865–3869.
[2] X. Zhao, M. Li, W. Sun, et al., Chem. Commun. 51 (2018) 7038–7041.
[3] K. Han, S. Wang, Q. Lei, J. Zhu, X. Zhang, ACS Nano 10 (2015) 10268–10277.
[4] J. Gao, J. Li, W. Geng, et al., J. Am. Chem. Soc. 140 (2018) 4945–4953.
[5] D. Ni, C.A. Ferreira, T.E. Barnhart, et al., J. Am. Chem. Soc. 140 (2018) 14971–14979.
[6] Q. Ma, X. Sun, W. Wang, et al., Chin. Chem. Lett. 33 (2022) 1681–1692.
[7] H. Jung, P. Verwilst, A. Sharma, et al., Chem. Soc. Rev. 47 (2018) 2280–2297.
[8] Y. Liu, P. Bhattarai, Z. Dai, X. Chen, Chem. Soc. Rev. 48 (2019) 2053–2108.
[9] X. Zhen, C. Xie, K. Pu, Angew. Chem. Int. Ed. 57 (2018) 3938–3942.
[10] R. Chen, J. Wang, H. Qiao, Prog. Chem. 29 (2017) 329–336.
[11] A. Turksoy, D. Yildiz, E.U. Akkaya, Coord. Chem. Rev. 379 (2019) 47–64.
[12] Y. Chen, Y. Su, S. Hu, S. Chen, Adv. Drug Deliv. Rev. 105 (2016) 190–204.
[13] Y. Yang, W. Zhu, Z. Dong, et al., Adv. Mater. 29 (2017) 28833643.
[14] K. Li, X. Duan, Z. Liu, et al., Nat. Commun. 12 (2021) 2376.
[15] Y. Wang, D. Zhang, K. Xiong, R. Shang, X.D. Jiang, Chin. Chem. Lett. 33 (2022) 115–122.
[16] D. Zhang, M. Xiong, Q. Yang, et al., Chem. Commun. 58 (2022) 10060–10063.
[17] X. Wang, Z. Jiang, Z. Liu, et al., Sci. Adv. 8 (2022) eadd5660.
[18] D. Wang, G. Wang, K. Liu, et al., Chin. Chem. Lett. 33 (2022) 2532–2536.
[19] P. Sun, Q. Wu, X. Sun, et al., Chem. Commun. 54 (2018) 13395–13398.
[20] W. Chen, C.A. Cheng, E.D. Cosco, et al., J. Am. Chem. Soc. 141 (2019) 12475–12480.
[21] C. Sun, B. Li, M. Zhao, et al., J. Am. Chem. Soc. 141 (2019) 19221–19225.
[22] S. Yagai, T. Seki, T. Karatsu, A. Kitamura, F. Würthner, Angew. Chem. Int. Ed. 47 (2008) 3367–3371.
[23] Z. Liu, Y. Zheng, T. Xie, et al., Chin. Chem. Lett. 32 (2021) 3862–3864.
[24] T. Zhang, X. Ma, H. Tian, Chem. Sci. 11 (2020) 482–487.
[25] T. Cheng, T. Wang, W. Zhu, et al., Org. Lett. 13 (2011) 3656–3659.
[26] F. Wang, Z. Guo, X. Li, X. Li, C. Zhao, Chem. Eur. J. 20 (2014) 11471–11478.
[27] H. Dai, Z. Cheng, T. Zhang, et al., Chin. Chem. Lett. 33 (2022) 2501–2506.
[28] B. Tian, S. Liu, L. Feng, et al., Adv. Funct. Mater. 31 (2021) 2100549.
[29] T. Sun, J. Dou, S. Liu, et al., ACS Appl. Mater. Interfaces 10 (2018) 7919–7926.
[30] W. Dou, F. Xu, C. Xu, et al., Chem. Sci. 12 (2021) 11089–11097.
[31] W. Sun, X. Zhao, J. Fan, J. Du, X. Peng, Small 15 (2019) 1804927.
[32] B. Hu, Z. Zhao, X. Gao, et al., J. Mater. Chem. B 9 (2021) 8832–8841.
[33] P. Gao, H. Wang, Y. Cheng, Chin. Chem. Lett. 33 (2022) 575–586.
[34] C. Ma, T. Zhang, Z. Xie, J. Mater. Chem. B 9 (2021) 7318–7327.
[35] Y. Xu, T. Feng, T. Yang, et al., ACS Appl. Mater. Interfaces 10 (2018) 16299–16307.
[36] X.D. Jiang, T. Fang, X. Liu, D. Xi, Eur. J. Org. Chem. 34 (2017) 5074–5079.
[37] D. Xi, M. Xiao, X. Peng, et al., Adv. Mater. 11 (2020) 1907855.
[38] Y. Su, Q. Hu, D. Zhang, et al., Chem. Eur. J. 28 (2022) 202103571.
[39] B. Zheng, Q. He, X. Li, J. Yoon, J. Huang, Coord. Chem. Rev. 426 (2021) 213548.
[40] J.R. Melamed, R.S. Edelstein, E.S. Day, ACS Nano 9 (2015) 6–11.
[41] M. Perez-Hernandez, P.D. Pino, S.G. Mitchell, et al., ACS Nano 9 (2015) 52–61.
[42] S.C. Lee, J. Heo, H. Woo, et al., Chem. Eur. J. 24 (2018) 13706–13718.
[43] L. Zhu, W. Lin, Sens. Actuators B: Chem. 352 (2022) 131042.
[44] W. Chi, Q. Qiao, R. Lee, et al., Angew. Chem. Int. Ed. 21 (2019) 7073–7077.
[45] L. Wang, Y. Xiao, W. Tian, L. Deng, J. Am. Chem. Soc. 135 (2013) 2903–2906.
[46] C.M. Krishna, Y. Lion, P. Riesz, Photochem. Photobiol. 45 (1987) 1–6.
[47] J.R. Kanofsky, Photochem. Photobiol. 87 (2011) 14–17.
[48] S. Atifi, M.N. Mirvakili, C.A. Williams, et al., Adv. Mater. 34 (2022) 2109170.
[49] F. Xia, A. He, H. Zhao, et al., ACS Nano 16 (2022) 169–179.
[50] C. Fan, T. Bian, L. Shang, et al., Nanoscale 8 (2016) 3923–3925.
[51] E.E. Jelly, Nature 138 (1936) 1009–1010.
[52] M. Zheng, P. Zhao, Z. Luo, et al., ACS Appl. Mater. Interfaces 6 (2014) 6709–6716.
[53] D. Gao, B. Zhang, Y. Liu, et al., Theranostics 9 (2019) 5315–5331.
[54] C.M. Hessel, V.P. Pattani, M. Rasch, et al., Nano Lett. 11 (2011) 2560–2566.
[55] Z. Wang, Cells 10 (2021) 3327.
[56] J. Hartl, P. Kiefer, A. Kaczmarczyk, et al., Nat. Metab. 2 (2020) 153–166.
[57] J. Lin, M.A. Milhollen, P.G. Smith, U. Narayanan, A. Dutta, Cancer Res. 70 (2010) 10310–10320.
[58] M. Hirayama, F. Wei, T. Chujo, et al., Cell Rep. 31 (2020) 107464.
[59] X. Feng, Y. Yu, S. He, et al., Cancer Lett. 385 (2017) 12–20.
[60] A.C. Timucin, H. Basaga, O. Kutuk, Med. Res. Rev. 39 (2019) 146–175.